Identify Similarities in Diverse Polycyclic Aromatic Hydrocarbons of Asphaltenes and Heavy Oils Revealed by Noncontact Atomic Force Microscopy: Aromaticity, Bonding, and Implications in Reactivity

Yunlong Zhang

Yunlong.zhang@exxonmobil.com

Corporate Strategic Research, ExxonMobil Research and Engineering Company,

1545 Route 22 East, Annandale, NJ 08801

Heavy oils are enriched with polycyclic (or polynuclear) aromatic hydrocarbons (PAH or PNA), but characterization of their chemical structures has been a great challenge due to their tremendous diversity. Recently, with the advent of molecular imaging with noncontact Atomic Force Microscopy (nc-AFM), molecular structures of petroleum has been imaged and a diverse range of novel PAH structures was revealed. Understanding these structures will help to understand their chemical reactivities and the mechanisms of their formation or conversion. Studies on aromaticity and bonding provide means to recognize their intrinsic structural patterns which is crucial to reconcile a small number of structures from AFM and to predict infinite number of diverse molecules in bulk. Four types of PAH structures can be categorized according to their relative stability and reactivity, and it was found that the most and least stable types are rarely observed in AFM, with most molecules as intermediate types in a subtle balance of kinetic reactivity and thermodynamic stability. Local aromaticity was found maximized when possible for both alternant and nonalternant PAHs revealed by the aromaticity index NICS (Nucleus-Independent Chemical Shift) values. The unique role of five-membered rings in disrupting the electron distribution was recognized. Especially, the presence of partial double bonds in most petroleum PAHs was identified and their implications in the structure and reactivity of petroleum are discussed.

1. Overview of the molecular characterization techniques

There is no more basic enterprise in chemistry than the determination of the geometrical structure of a molecule. Such a determination, when it is well done, ends all speculation as to the structure and provides us with the starting point for the understanding of every physical, chemical and biological property of the molecule.

The fundamental principle of *structure determines function* is well reflected by the eloquent and much quoted statement above by Roald Hoffmann.[1] Characterizing the structure of organic molecules has been a major effort for chemists for centuries since the tetravalency of carbon was put forward by van't Hoff in1874 and the structure of benzene by Kekulé in 1875.[2] For many decades, researchers have deduced molecular structure from indirect methods.[3] For example, elemental analysis provides elemental composition, UV-vis spectroscopy depends on absorption of conjugated systems, and vibrational spectroscopy (FT-IR and Raman) identifies functional groups. Mass spectrometry is a valuable tool for elucidating molecular formulas, and x-ray crystallography has revealed molecular conformation when pure crystals can be obtained. For cases where structural characterization is tremendously complicated, chemists often have to rely on chemical synthesis to ultimately confirm the structures.[4] Major breakthroughs followed with the introduction of NMR spectroscopy, which provides connectivity in covalent structures. However, most of these tools demand high purity samples of the material to be characterized, and/or larger amounts. The crucial role of purification cannot be overstated, as the well-known saying by Isaac Asimov that *The first step in making rabbit stew is catching the rabbit*. Thus, the chromatography techniques (GC, HPLC), either alone or in tandem with other tools (GC-MS, LC-MS, LC-NMR), have played instrumental roles in providing pure samples for characterization.

Chemists have longed for direct confirmation about what molecules might actually look like, and hoped to someday see molecular structures directly.[5] Recently this hope has become a reality via atomic-resolution molecular imaging techniques. Molecular imaging conventionally refers to techniques which use fluorescence microscopy to reach beyond the diffraction limit of optical microscopy, sometime even at molecular resolution.[6-8] Recently, this concept has been vastly expanded with the introduction of Cryogenic Electron Microscopy (cryo-EM), which was awarded the 2017 Nobel Prize in Chemistry. Cryo-EM enables atomic resolution for a variety of biological macromolecules and assemblies,[9-10] and the aberration corrected cyro-EM can potentially even reach sub-angstrom resolution.[11-14] Although used primarily for the backbone structure of biological macromolecules, cryo-EM has recently been applied to small organic compounds with microED (electron diffraction), with atomic-resolution (<1 Å) crystal structures obtained from nanocrystals ($\sim 10^{-15}$ g) in minutes.[15-16]

A different technique to obtain sub-atomic resolution of small organic molecules is scanning tunneling microscopy (STM) and atomic force microscopy (AFM). Both are scanning probe microscopy (SPM) technique and will be the focus of discussion in this paper. Unlike EM, which uses electrons as the probe, SPM uses a sharp metallic tip to probe the atoms. The original demonstration of chemical structure of small organic molecules such as pentacene was obtained with noncontact atomic force microscopy (nc-AFM) by Gross et al. in 2009.[17] Their unprecedented atomic resolution (up to 0.03 Å) was achieved using a carbon monoxide-functionalized tip.[17-18] Because of the vanishingly small samples (mg to μg) needed, and the low requirements for purity,

this direct molecular imaging AFM/STM technique is positioned as an ideal analytical method to characterize molecules in complex heterogeneous mixtures such as heavy petroleum.

2. Introduction to molecular imaging with STM/nc-AFM:

Scanning Tunneling Microscopy (STM) was invented by Binnig and Rohrer in 1982 and recognized with the Nobel Prize in Physics in 1986.[19] But STM does not allow for imaging molecular structure directly because the STM topology reflects the local density of states between two conductive phases. Atomic Force Microcopy (AFM) was introduced by Binnig, Quate, and Gerber in 1986, and operates by measuring the frequency shift of an oscillating cantilever which reflects the interaction forces.[20] This powerful technique has been widely used in studying the surface of materials on from micro- to nanometer scales.[21] However, most of these conventional AFM techniques are operated under either tapping or contact mode in which the cantilever tip is in contact with the sample. The noncontact mode nc-AFM was enabled by the invention of qPlus sensor by Giessibl et al. Here the oscillating amplitude can be controlled down to 0.1 angstroms.[22] Recently, the revolutionary breakthrough of imaging a small organic molecule directly was achieved by Gross et al. with a CO-functionalized probe tip.[17] Density functional theory (DFT) analysis attributed the high resolution of molecular structure in AFM to Pauli repulsion. A numerical Probe Particle Model developed by Hapala et al. reproduced the high resolution AFM and STM molecular images very well and demonstrated that the origin of the sharp image is due to strong lateral (not vertical) relaxation of the probe molecule attached to the metallic tip apex, and not from increased electron density attributable to any kind of chemical bonds.[23-24] However, other researchers consider it still controversial, and the contrast mechanism remains an active area of research.[25]

Real sub-atomic resolution images of organic molecules has be achieved by tips functionalized with Cl, Br, I, Ag, CO, and NO, although the CO tip (oxygen on the apex) seems to be especially robust and sensitive. It was soon further demonstrated that bond orders in buckminsterfullerene (C_{60}) could be distinguished with a resolution of 2 pm.[18] It has also been applied to characterize organic molecules from natural products[26] which could not be characterized directly with conventional methods such as NMR spectroscopy and mass spectrometry. For characterization of unknown structures, it is helpful to image the frontier molecular orbitals on two monolayers of insulator NaCl (2 ML) with STM and to compare these STM images with quantum chemical calculations of hypothesized candidate structures. This ultrahigh resolution technique has been demonstrated in monitoring a chemical reaction by direct imaging of covalent bond structure,[27] inducing chemical reactions,[28] and even imaging molecules at room temperature.[29] Two dimensional structures have been studied, such as the water network,[25] and hydrogen-bonded molecular clusters.[30]

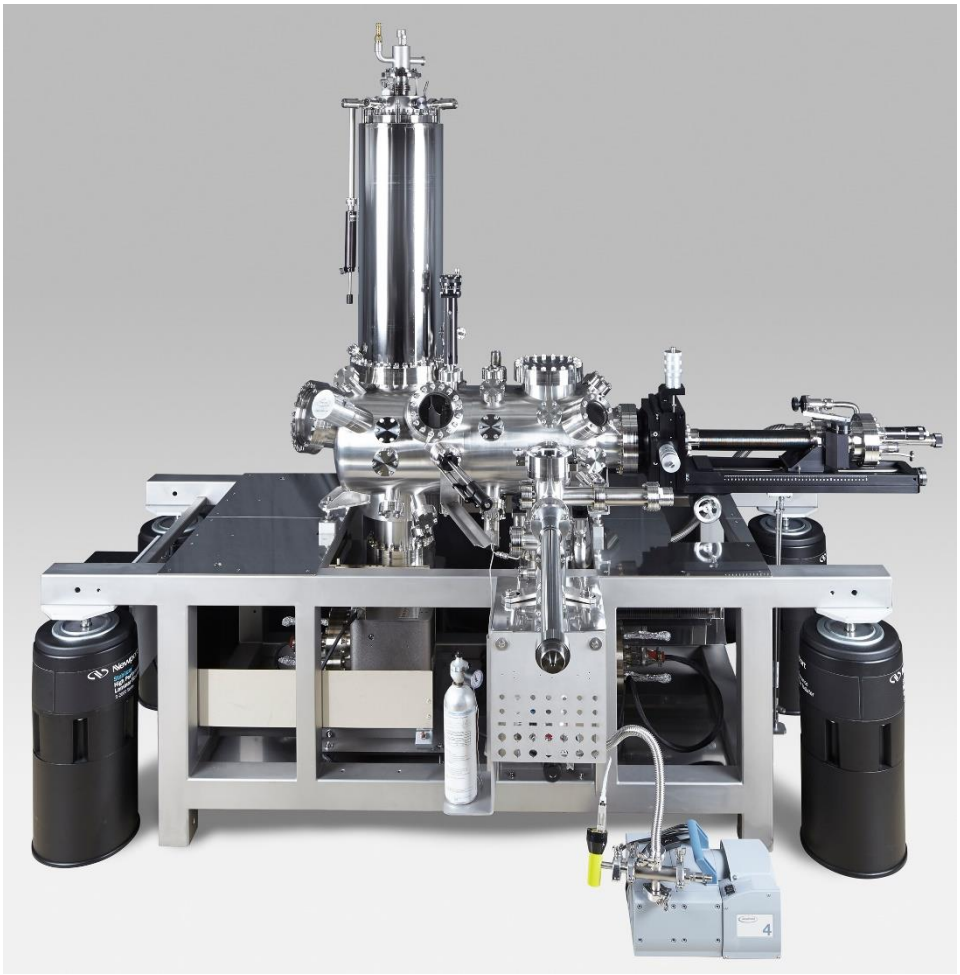

Figure 1. A picture of LT UHV STM/AFM for imaging organic molecules with functionalized CO-tip. (Picture credit by CreaTec Fischer & Co. GmbH)

A photo of a bimodal LT UHV STM/AFM instrument is shown in **Figure 1**. The cryo stage is operated at 4.7 K cooled by liquid helium surrounded by liquid nitrogen (77 K) to achieve ultralow temperature and prevent thermal diffusion. Ultrahigh vacuum (~10^{-10} mbar) is required to maintain the atomically clean system. The substrate is typically Cu (111), although Ag (111) and Au (111) can also been used. When preparing the system, single crystal Cu (111) is initially sputtered with Ar^+ for several cycles to remove any defects or contaminants. If needed, NaCl is deposited by subliming at room temperature or under slight heating to achieve a moderate coverage of one or multiple layers of NaCl. At cryo temperature (4.7 K), carbon monoxide (CO) is doped and functionalization with a CO tip is achieved by picking up an individual CO molecule.[31] Typically a sample is prepared by flash heating a sample deposited onto the silicon wafer via resistive heating.

Major advantages of nc-AFM include: (1) bond-like structures and sub-atomic resolution of molecular structures, (2) atomic manipulation using the tip to move molecules or even break bonds, (3) sensitivity to adsorption geometry on a metal (catalyst) surface, (4) imaging of individual molecules requiring very small sample size (micrograms) and with a low purity

requirement, (5) low temperature (4.7 K) and ultrahigh vacuum to preserve reactive intermediates and to prevent most chemical reactions.

Despite these features and advantages, there are significant challenges and disadvantages to using nc-AFM. Imaging molecules one by one requires maintaining cryogenic conditions and instrument stability for periods from hours to days. Several days are typically required to prepare the sample and tip. The acquisition time for an AFM image of an individual molecule is typically 15-30 min. Like any surface technique, planar molecules are preferred over nonplanar and three-dimensional structures, although recently a few nonplanar molecules have been studied. Sample preparation by flash deposition limits the molecular weight of most studied molecules to ~1000 Dalton. The high resolution is achieved only at cryogenic temperature where reaction dynamics might be frozen out.[32] Identification of heteroatoms is difficult and interpretation of images is mostly by visual assessment rather than computer algorithms, due to the lack of model systems. Aggregation phenomena and other bulk interactions on cryogenic surfaces are poorly understood.

To address these challenges, an initial study on the aliphatic moieties in aromatic molecules was performed.[33] Model compounds allowed benchmarking of the sample preparation conditions, especially the effect flash vaporization vacuum cryo-deposition on the structural integrity of the molecules bonds. This integrity, and establishing that the vaporization did not introduce sampling bias in the representativeness of detected molecules (for example, as a function of molecular weight), was essential in qualifying the sample preparation methods for the study of heterogeneous petroleum mixtures.[34] Other preparation methods such as electrospray deposition would allow deposition of molecular weights larger than 1000 Daltons.[35]

So far there are a few papers published on imaging petroleum molecules and related samples such as coal and petroleum asphaltenes (2015),[36] a heavy oil mixtures and asphaltenes (2017),[37] and more recently on fuel pyrolysis products (2018)[38] and marine dissolved organic matters (2018).[39] Understanding these molecules has been challenging, except in one initial study which sought to find the common structural patterns and to connect a limited number of diverse molecules (each one different) to the infinitely large number of these molecules in a bulk sample.[40] A more systematic analysis of such AFM structures is described below.

3. Computational Details

Theoretical computations on the AFM structures were performed with density functional theory (DFT) as implemented in Gaussian 09 Revision D.01.[41] Becke's three-parameter hybrid exchange functional with the Lee−Yang−Parr correlation functional (B3LYP) were used.[42-43] Geometries were optimized with B3LYP and 6-31+G(d,p) basis sets, and vibrational frequency calculations on the optimized geometries were performed at the same level of theory to characterize all stationary points as minima. All calculations were in the gas phase. NICS values as an aromaticity index were obtained from NMR calculations with the GIAO (Gauge-Independent Atomic Orbital) method at the level of B3LYP/6-31+G(d,p), and the negative values of the magnetic shielding (chemical shifts) of dummy atoms (Bq) placed one angstrom above the center of each ring were used.[44] Electrostatic potential surfaces (ESPs) were computed using the cubegen function in Gaussian and results were visualized with GaussView5.0.8. UV-vis spectra were predicted with TD-DFT calculations at B3LYP/6-311+G(d,p) by allowing 20 excited states transitions.

Population analysis was performed with the natural bond orbital (NBO) program version 3.1[45-47] under the Gaussian09 program package, and the widely used Wiberg bond index (WBI) is reported as the bond order.[48]

4. Results and Discussions

4.1. Overview of the AFM structures

The structures observed in heavy oils are reproduced below in **Figure 2.** Some ambiguities in originally assigned structures from AFM images have been omitted for clarity and the reader should refer to the original publications by Schuler et al. for more accurate information on their chemical structures and for sample descriptions.[37]

This analysis focuses on polycyclic (or polynuclear) aromatic hydrocarbons (PAHs or PNAs) since they are observed in many of the heaviest petroleum-derived organic molecules. In the original 2015 JACS paper on asphaltenes,[36] 32 chemical structures of coal asphaltene molecules were assigned among the 100 images from coal samples, and only one structure from a petroleum asphaltene was assigned among the 15 images obtained for the petroleum asphaltene sample, indicating the greater extent of nonplanar molecules in petroleum. In the 2017 Energy & Fuels paper by Schuler et al.,[37] a total of 104 structures were reported for a total of 382 images obtained, with 17 structures for 65 images of A1, 16 structures for 62 images of A2, 12 structures for 49 images of B1, 10 structures out of 34 images of B2, 39 structures out of 68 images of C1, 3 structures out of 30 images of C2, 2 structures out of 36 images of D1, and 5 images out of 38 images of D2 sample. Overall, a total of 137 structures (28%) have been assigned among the 497 images obtained in these two publications. This shows that a large number of images remained unassigned and illustrates the challenge of assigning the remaining chemical structures to AFM images of petroleum by visual inspection. We envision that computer algorithms utilizing artificial intelligence and pattern recognition will play a role in assigning structures for unknown samples in the future.

C1.1

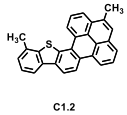
C1.2

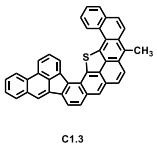
C1.3

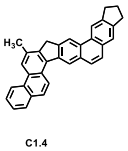
C1.4

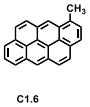
C1.6

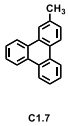
C1.7

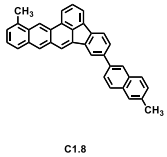
C1.8

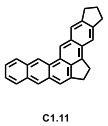
C1.11


C1.13

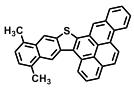
C1.17


C1.19


C1.20

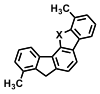
C1.26

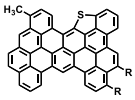
C1.27

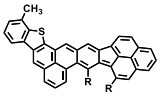
C1.28

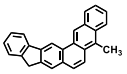
C1.29

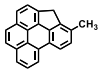
C1.31

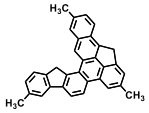
C1.32

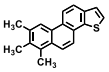
C1.34

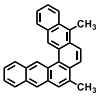
C1.35

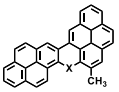
C1.36

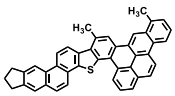
C1.37

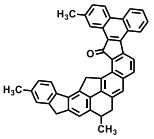
C1.40

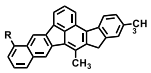
C1.43

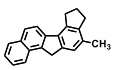
C1.45

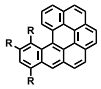
C1.47


C1.48

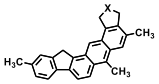
C1.49


C1.50


C1.52

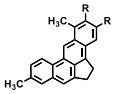
C1.53

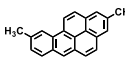
C1.55

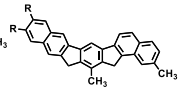
C1.58


C1.59

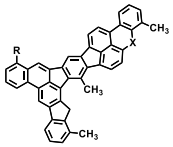
C1.62


C1.63

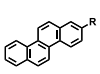
C1.66

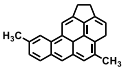
C1.67


C2.1

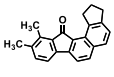
C2.2

C2.12

C2.23

C2.27

D1.6

D1.9

D2.3

D2.5

D2.10

D2.13

D2.14

D2.19

A1.1

A1.3

A1.4

A1.5

A1.6

A1.9

A1.10

A1.14

A1.16

A1.22

A1.26

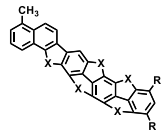

A1.29

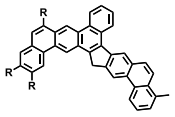

A1.41

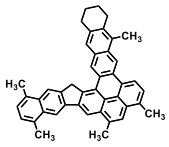

A1.43

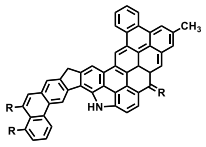

A1.47

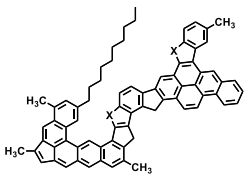

A1.52

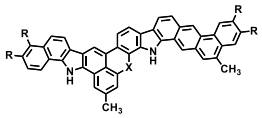

A1.56

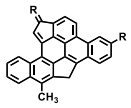

A1.57

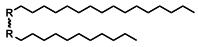

A2.1

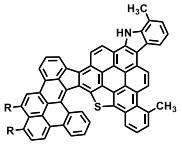

A2.2

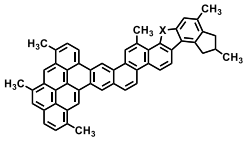

A2.3

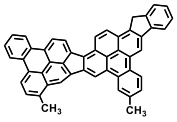

A2.6

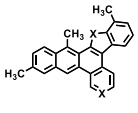

A2.9

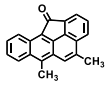

A2.13

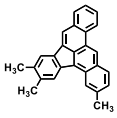

A2.14

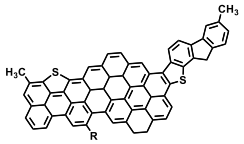

A2.17

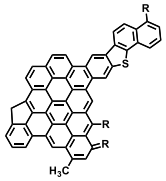

A2.18

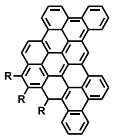

A2.19

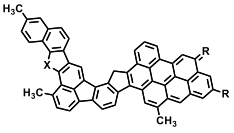

A2.20

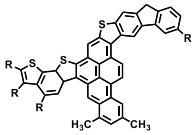

A2.25

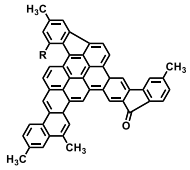

A2.27

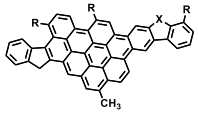

A2.30

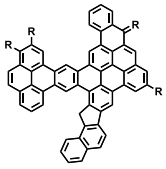

A2.31

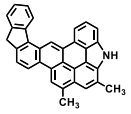

A2.49

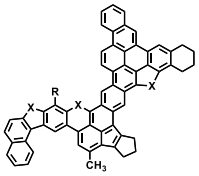

A2.53

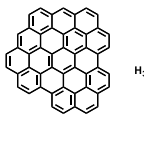

B1.1

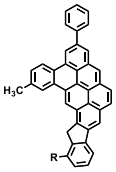

B1.2

B1.3

B1.4

B1.5

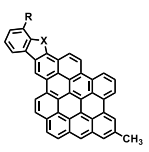

B1.6

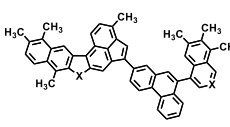

B1.7

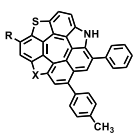

B1.10

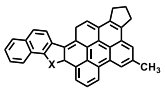

B1.19

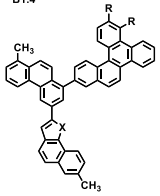

B1.25

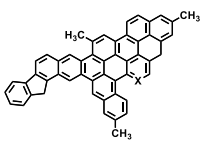

B1.27

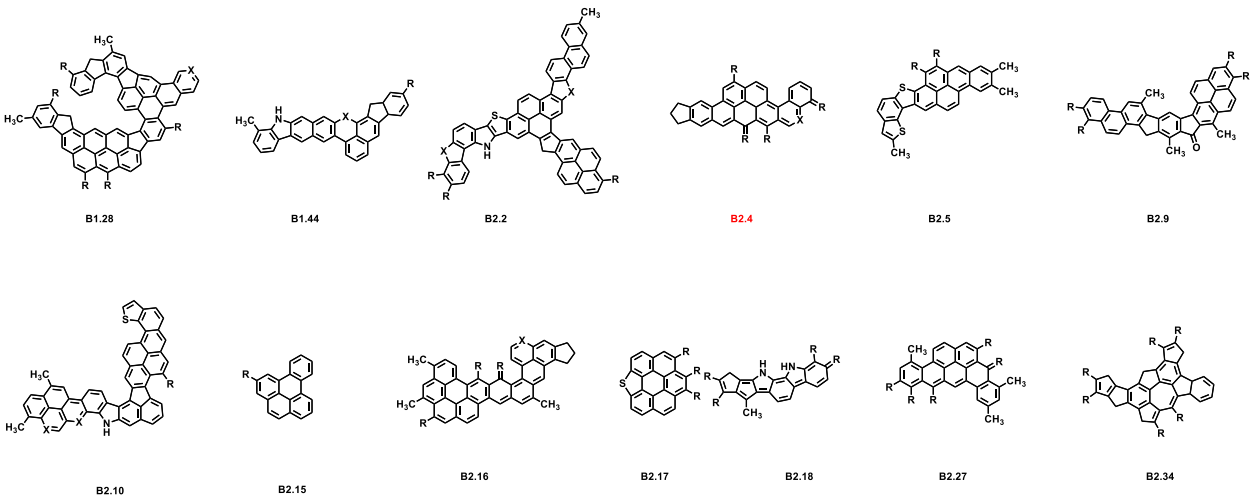

Figure 2. Chemical structures of petroleum molecules from AFM imaging. Reprinted with permission from Ref. [37]. Copyright 2017 American Chemical Society.

4.2. Understanding the molecular geometries of PAHs

These detailed structures from AFM were studied to understand their conformations and geometries by using density functional theory (DFT) and their structures were shown in **Figure 3**. Although most of these molecules are planar or semi-planar PAH molecules, some nonplanar moieties are present, and even a few helical structures are observed (C1.3 and C1.36). These indicate that strong interaction with substrate (Cu 111) play an important role and the substrate could induce some conformational planarity in structures. It is important to notice that heteroatoms are frequently observed within the "cove" area, buried inside of the structures (C1.3, C1.2, C1.36, and C1.27). Molecule C1.3 is an extreme case because the internal S atom is also "sandwiched" between the two helical moieties, making it inaccessible from all directions. This steric hindrance accounts for the difficulty in removing the heteroatoms under hydroprocessing conditions.

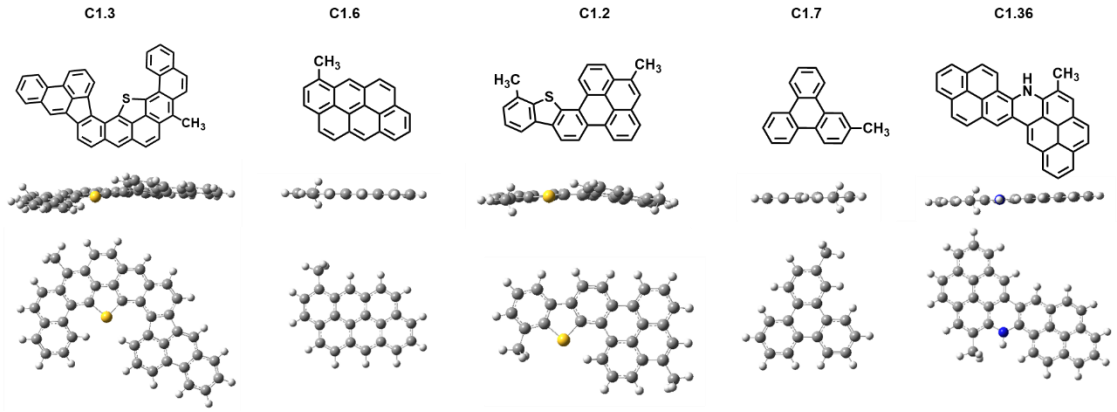

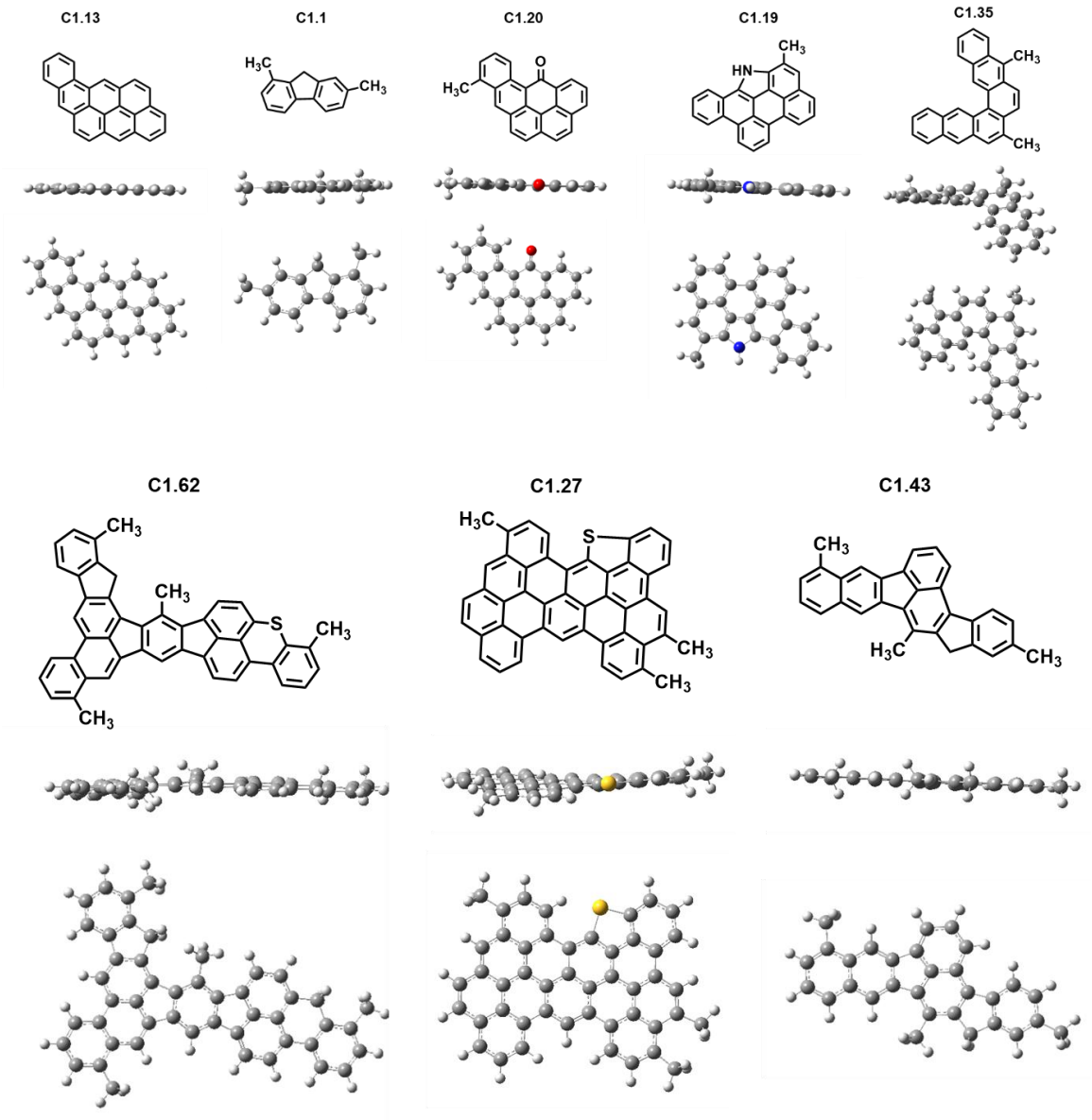

Figure 3. Representative detailed molecular structures from AFM imaging with geometries optimized with DFT calculations. The chemical structure, along with the side and top views show the conformations of each structure.

It is a significant point that five-membered rings are frequently observed in many of these molecule, and sometimes even seven-membered rings are observed. The molecular geometries of PAHs can be classified as alternant and nonalternant hydrocarbons (**Figure 4**). The best way to check whether a PAH is alternant or nonalternant is to use the star-unstar approach. Starting with any carbon atom by putting a star in the molecule and going around the ring alternating putting stars, if at the end, two atoms are next to each other that are starred (or unstarred), the molecule is nonalternant. There are important differences among these structural isomers. For example, despite sharing the same $C_{10}H_8$ formula, nonalternant azulene is blue while naphthalene is colorless. Pyrene and fluoranthene share the same formula ($C_{16}H_{10}$, **Figure 4**), but the nonalternant fluoranthene fluoresces strongly, and differently, than its isomeric alternant pyrene. While

alternant molecules have mirror-related bonding and antibonding orbitals, nonalternants do not have mirror-related orbitals, resulting in nonzero charges on some atoms and a different electron distribution.[49] Therefore, nonalternant hydrocarbon are significant because of many unusual electronic properties they exhibit, such as large dipole moments, long fluorescence lifetimes, UV-vis light absorption, and high electron affinities.

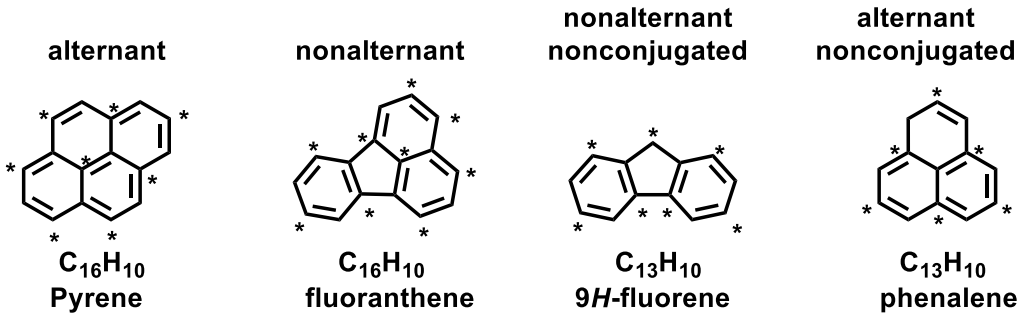

Figure 4. Classification of nonalternant and alternant polycyclic aromatic hydrocarbons by the starring approach.

Many structures observed by AFM imaging in **Figure 2** are new molecules and have never been discovered in the literature. Most of them are alternant, but nonalternants are also observed. These two isomers cannot be easily distinguished by conventional techniques such as NMR or MS. This indicates that other techniques, such as fluorescence or UV-vis, might be valuable to consider for quantifying their presence. The significance for the distinction of alternant and nonalternant hydrocarbons, and the presence of nonalternant PAH will be discussed in more detail below. Calculations (**Figure 3**) predicted and confirmed that hydrocarbon molecules containing a five-membered ring without heteroatoms have a larger dipole moment and become a more polar molecule, e.g. compound C1.43 (1.22 Debye). As expected, heteroatoms contribute significantly to the polarity of molecules, such as molecules C1.36 (2.67 Debye, N), C1.20 (2.32 Debye, O), C1.19 (2.32 Debye, N), and C1.62 (2.13 Debye, S).

A second type of nonconjugated nonalternant hydrocarbons are also observed, such as fluorene with a CH_2 bridge between two aromatic rings (**Figure 4**). It should be noted that fluorene has an odd carbon number and the fully conjugated isomer ($C_{13}H_{10}$, phenalene) has a non-Kekulé structure. Some free radical species have been observed from the distinctive singly-occupied molecular orbital or SOMO[36] of these free radicals (e.g., CA12) as imposed by its geometry, *i.e.,* a fully conjugated aromatic system is not possible with an odd carbon number PAH. Unless the geometry of molecules was thermally altered or structurally rearranged, these free radicals were very likely native free radicals. The presence of stable free radical species in native asphaltenes has been reported since the1960s,[50] when free radicals were detected by electron spin resonance (ESR) spectroscopy and remained a subject of active research.[51-52] Therefore, detection of these odd-carbon number PAHs might provide a clue to the presence of these types of free radicals and their structures.

It is helpful to understand the structure of these PAHs within the context of hydrocarbon spaces. For polycyclic aromatic hydrocarbons (PAHs) composed of six-membered rings only, the maximal number of topological structures is based on polyhexes in mathematics. The form of polyhexes can be enumerated for a certain number of hexagonal rings (R) by 1 (1R), 1 (2R), 3

(3R), 7 (4R), 22 (5R), 82 (6R), 333 (7R), 1448 (8R), 6572 (9R), and 30490 (10R). Therefore, the number of possible structures for a molecule composed of ten hexagonal rings can easily reach ~30,000. Computer algorithms have been developed and the enumeration of benzenoid hydrocarbons has reached ~ 5.8×10^{21} for 35 fused benzene rings.[53] It should be noted that although not all predicted polyhexes are reasonable chemical structures. In this aspect, Dias prepared periodic tables by enumerating possible chemical isomers for each formulas,[54-60] and in later studies with five-membered rings incorporated,[61] and correlation of relative energetics and stabilities with structures.[62]

4.3. Energetics and stability of PAHs

Aromaticity can be considered to impart increased stability at the loss of olefin reactivity. Although its electronic nature is often associated with 4n+2 π electrons by Hückel's rule, it was only intended for monocyclic systems such as benzene and annulene.[63] For polycyclic aromatic hydrocarbons (PAHs), only two-ring (naphthalene, $C_{10}H_8$) and three-ring aromatic hydrocarbons (phenanthrene and anthracene, $C_{14}H_{10}$) are consistent with 4n+2 rule, while most other PNAs larger than three rings do not follow this rule (**Figure 5**). For example, pyrene has 16 π electrons and coronene has 24 π electrons, making them antiaromatic according to Hückel's rule. To extend Hückel's rule to PNAs, the Platt's perimeter model (which traces only the peripheral carbons) was developed.[64] With this modification, pyrene (14) and coronene (18) are now consistent with the 4n+2 rule. More recent models describing the aromaticity of PAHs include the Randić's Conjugated Circuit (CC) Model.[65]

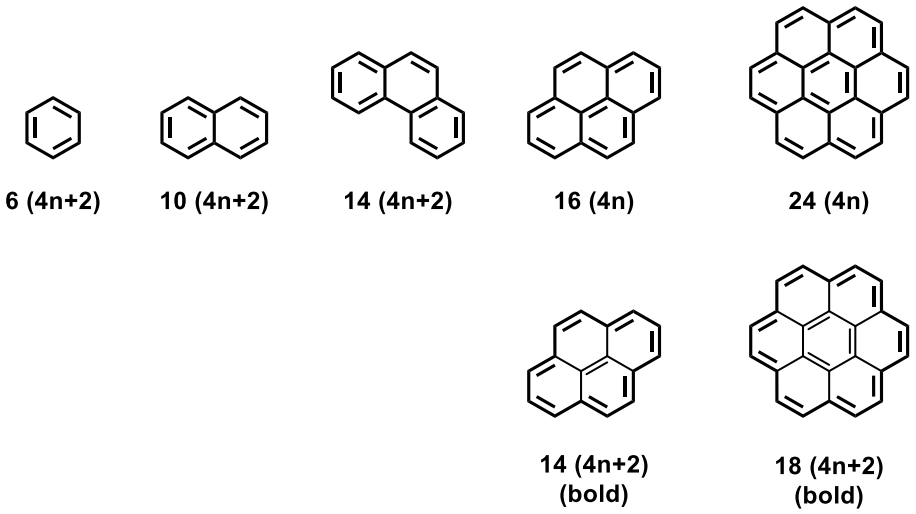

Figure 5. Electron counting rules for describing aromaticity of monocyclic (benzene) is different with PAHs. The Hückel's 4n+2 rule applies for monocyclic system (such as benzene) only, and cannot be used for PAH. The addition of Platt's perimeter rule (by tracing only the peripheral carbons, shown in bold) make PAH consistent with 4n+2 rule.

The relative energetics and stabilities of PAHs are related to the Kekulé structures. For example, the Hull's rule states that the greater the Kekulé structure count, the greater is the thermodynamic stability of a benzenoid hydrocarbon. Clar's sextet theory is the most prominent theory for benzenoidal PAHs and has received widespread application. Clar's sextet rule states that the Kekulé resonance structure with the largest number of disjoint π-sextets is the most

important to characterize properties of PAHs.[66] Aromatic π-sextets were defined by Clar as six π-electrons localized in a single benzene-like ring separated from adjacent rings by formal C–C single bonds. With this theory, it is easy to understand the decreased stability (increased reactivity) with increasing number of rings in polyacenes. For example, hexacene (6-linear annulated benzene rings) is unstable to both light and air.[45] Calculations confirmed that the singlet-triplet band gap of polyacenes decreases as the system size increases, and reaches zero for 9, meaning the most stable form of polyacene for n = 10 is essentially a biradical.[67] These predictions have been confirmed by the recent experimental work on heptacene at ~150 K,[68] and the synthesis of polyacenes on a gold surface with STM.[69] By examining the structures shown in **Figure 2**, it is important to notice that the maximal number of linear rings in petroleum molecules is three, and a kink or turn is found whenever the linear rings reaches three, which we dubbed the *Rule of Three* **(Figure 6)**, indicating a fine interplay between the kinetic reactivity and thermodynamic stabilities of these PAH molecules found in petroleum structures. Recently it has been shown that the relative stability of kinked vs. straight topologies in PAHs is driven by aromaticity.[70]

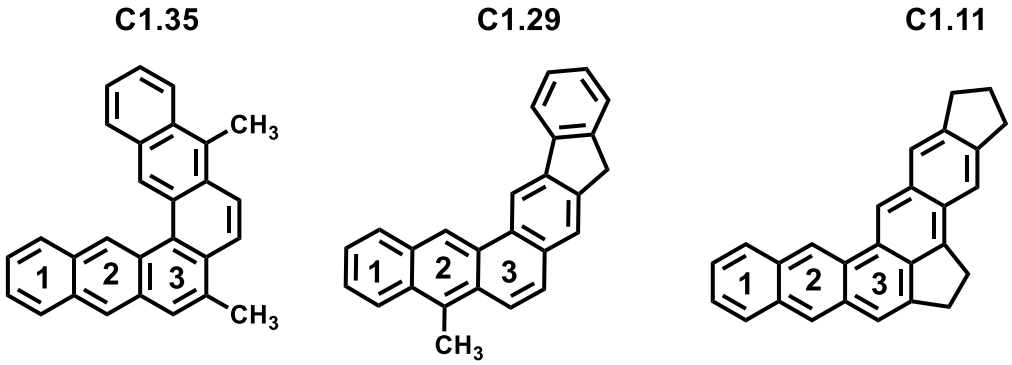

Figure 6. Petroleum structures identified with AFM imaging have three or fewer linear rings.

Clar's π-sextet rule can be applied only to PAHs having six-membered rings (6-MRs), i.e., benzenoid species. Glidewell and Lloyd proposed to extend the Clar rule to non-benzenoid PAHs containing four- and eight-membered rings which is later known as the Glidewell-Lloyd rule.[63] Relative stabilities of PAHs can be analyzed with these theories, and it has been empirically categorized based on reactivities and stability,[65] and three types of structures has been categorized.[65, 71] For example, the most stable type of molecules are those having only one Clar's structure composed of only sextets and empty rings (indicated by inscribed circles, D in **Figure 7**), such as triphenylene and hexabenzocoronene (which has a melting point much higher than the glass tubes used to measure melting point),[66] and they were termed *fully benzenoids* by Clar,[66] or *total resonant sextet* (TRS) by Dias, or *all-benzenoid* by Cyvin and Gutman, or *fully aromatic* by Randić.[71] The next most stable are those benzenoids with several Clar structures (i.e, C), and benzenoids with only one Clar structure with a fixed sextet and double bonds are next least stable (phenanthrene and pyrene, B).[65]

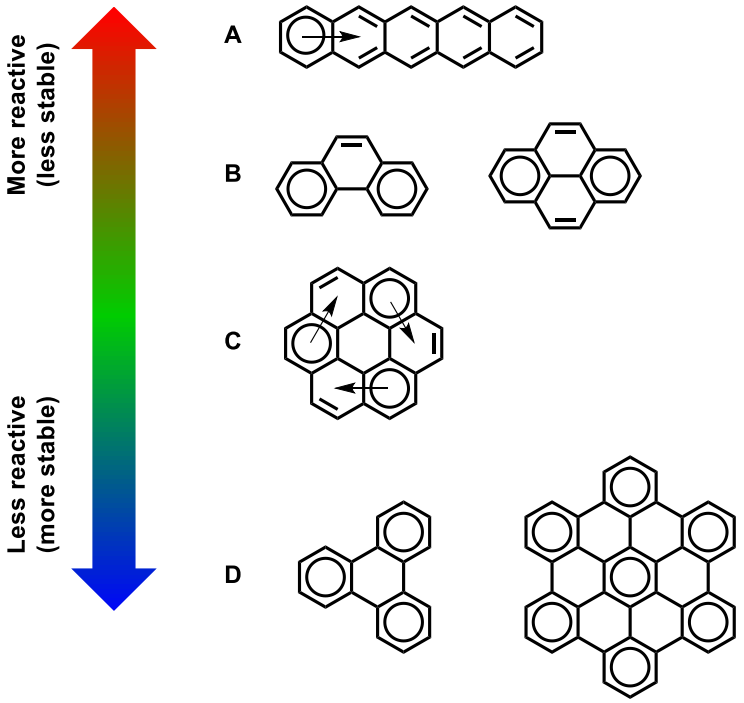

Figure 7. Stabilities of PAHs predicted by Clar's sextet theory.

However, since the least stable are polyacenes with only one sextet (A), four types of PAHs can be distinguished by modifying the previous three PAH classes (**Figure 7**). Based on this analysis and the observed structures in Figure 2, it is found that the most stable (D type) and least stable (A type) structures are very rare (the only exception is triphenylene), and that most of them are consistent with intermediate B and C types. This initial analysis can be used to study other structures.

4.4. Local aromaticity of PAHs

According to the IUPAC Gold Book,[72] aromaticity is defined as *the concept of spatial and electronic structure of cyclic molecular systems displaying the effects of cyclic electron delocalization which provide for their enhanced thermodynamic stability (relative to acyclic structural analogues) and tendency to retain the structural type in the course of chemical transformation.* Aromaticity is a typical example of a unicorn in chemistry; as a popular concept in chemistry everybody seems to know what it means although it is just a virtual quantity rather than experimentally observable.[73] There are many indices to quantify aromaticity based on various criteria. The well-known indices based on energetics include: Dewar Resonance Energy (DRE, 1965), Total Resonance Energy (TRE, 1976), and Aromatic Stabilization Energy (ASE). The structural indices include: HOMA, EN, and GEO.[74-75] The electronic distribution indices include: PDI and FLU. Finally the indices based on magnetic shielding include: TRC, ARCS, CDA, and NICS.[76]

Local aromaticity can be conveniently assessed using the aromaticity index NICS (nucleus-independent chemical shifts),[44] which is a measure of local aromaticity of each ring of a PAH including both alternant and nonalternant PAHs.[77-79] Enabled by this magnetic index, the

continuous aromaticity spectrum can be classified from aromatic to nonaromatic to antiaromatic according to the computed NICS value for a few typical PAHs (**Figure 8**).

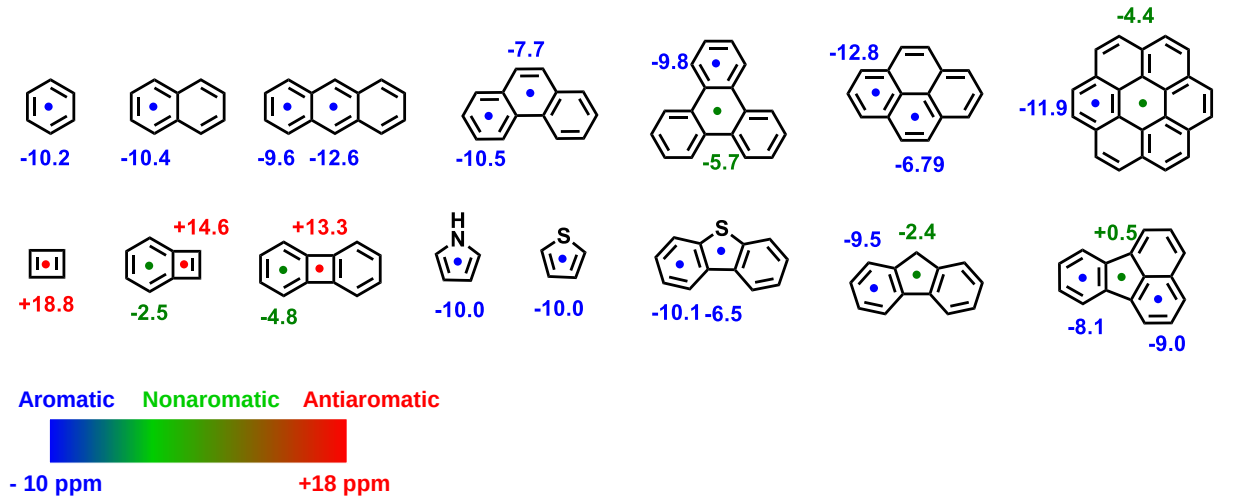

Figure 8. The local aromaticity calculated with NICS(1) in ppm (one angstrom above the center of each ring) computed with B3LYP/6-311G(d,p). Color schemes are relatively more aromatic in blue, nonaromatic in green, and more antiaromatic in red.

As a benchmark, the chemical shifts calculated at the center of aromatic benzene is -10.2 ppm, and antiaromatic cyclobutadiene is +18.8 ppm. The aromaticity in naphthalene and anthracene is expected, although more aromatic character (decrease in chemical shift) predicted at the middle ring of anthracene is a known issue for this method and has been extensively discussed. In phenanthrene, the middle ring (-7.7 ppm) has decreased aromaticity vs. the two side rings (-10.5 ppm), as expected from Clar's sextet theory. Similarly, NICS calculations for other PAHs (triphenylene, pyrene, and coronene) are also precisely consistent with predictions by Clar's rule. Furthermore, the decreased aromaticity character due to annelation with antiaromatic cyclobutadiene are also correctly predicted. Although thiophene and pyrrole are predicted to be aromatic, it is interesting to note the S-containing central ring of the aromatic dibenzothiophene is nonaromatic, with a magnitude comparable to the middle rings of pyrene. Based on this, it is not surprising to see that the nonconjugated five-membered ring of fluorene (- 2.4 ppm) has little aromatic character, since it is equivalent to a CH_2 bridged biphenyl molecule. However, the conjugated five-membered ring in fluoranthene is even less aromatic (+ 0.5 ppm) than of the nonconjugated fluorene. It indicates the significance and unusual behavior due to the presence of a central five-membered ring in nonalternant hydrocarbons observed in petroleum. It showed that the presence of a five-membered ring functions as a divider in a PAH prevents the delocalization of electron density in the molecule. Taking together the predictions of the alternant benzenoids with Clar's theory and the nonalternant PAHs with NICS, it suggests that in polycyclic aromatic systems, rather than delocalization, the electron density in a PAH is localized and the conjugation is avoided, which is dramatically different with the conventional view in simple organic molecules that conjugation (or delocalization of electron density) is often considered as favorable and lower in energy. For this reason, we dub it as *selfish aromatics.* It should be noted this generalization in both alternant and nonalternant PAH is consistent with the Glidewell-Lloyd rule[80] and recent studies on individual systems.[63, 81]

4.5. Electronic structure and electron density distributions in PAHs

One major difference between nonalternant and alternant PAHs is the electron density distribution. While alternant hydrocarbons such as naphthalene, pentacene, pyrene, and coronene are normal type and have symmetric charge distributions, nonalternant PAHs such as azulene and fluoranthene have noticeable charge accumulation, as indicated by the electrostatic potential surface on the electron density plots (**Figure 9**). Compared to naphthalene, with its relatively even distribution among the two rings, significant charge separation among the two rings of azulene is noticed, with negative charges accumulated in the five-membered ring, and positive charges accumulated in the seven-membered rings. This non-even charge distribution is also evident in nonalternant fluoranthene, with positive charge distribution in the five-membered ring. Based on this, it is reasonable to understand the presence of five-membered rings in nonalternant PAH structures in petroleum molecules. The significant charge separation will provide a driver for larger than usual intermolecular van der Waals forces and even charge transfer between among aggregation of petroleum asphaltene molecules.[82]

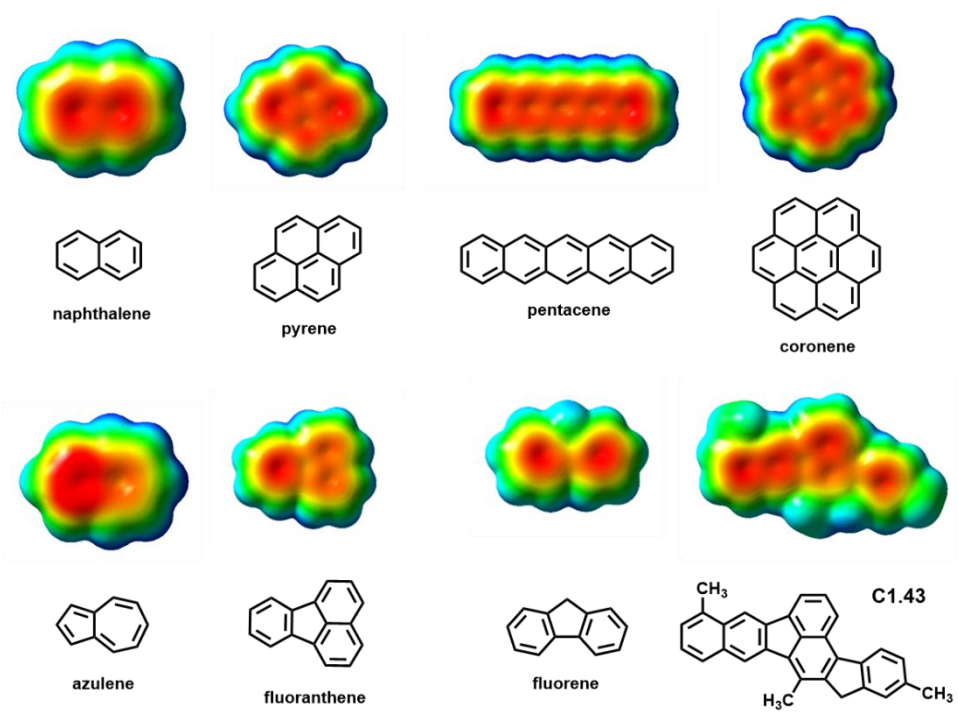

Figure 9. Electrostatic potential surfaces (isovalue 0.004) mapped onto the electron density plot (isovalue 0.02), with color schemes as negative in red and positive in blue.

4.6. UV-vis absorption

UV-vis spectroscopy is a great tool to study aromatic molecules, not only because UV-vis spectrometers are readily available, but because the electronic transition measured by UV-vis is related to the electronic structure of conjugated π systems. The abundant aromatic molecules in petroleum manifest themselves by the canonical black color crude oils, and the origins for the black of color of most heavy oils, resids, and asphaltenes has been extensively studied.[83-84]

Although crude oils of other colors (e.g., blue oil [85]) has been reported, it was shown to be due to the fluorescence emission by perylene, indicating the multifaceted reasons for the apparent color of petroleum. It is understandable that heteroatom enrichment in these fractions plays an important role in the optical spectra, but the role of PAHs (or aromatics) is also significant to the light absorption in the visible range, and has been treated extensively.[86] In his classic book *The Aromatic Sextet* (1972),[66] Clar examined numerous compounds and their UV-vis absorption and some of them are listed in **Figure 10**. It can be seen that these stable PAHs of up to five, six, seven, or even more fused rings with more sextets could not absorb much visible light, and hence would appear light color or colorless. Hence Clar reasoned that the dark color of graphite must appear very late (i.e., much larger number of rings).[66] Later the Urbach tail (Urbach energy), which was commonly encountered for the light absorption below the band gap of semiconductors (B region),[87] was involved for the long-wavelength light absorption of asphaltenes.[86] More detailed studied focused on the long-wavelength absorption > 600 nm indicated that the large PAHs (up to 15 rings) and decreasing sextet carbon fractions were identified as the key contributors by MO calculations on hundreds of alternant (six-membered rings) PAHs.[83-84, 88]

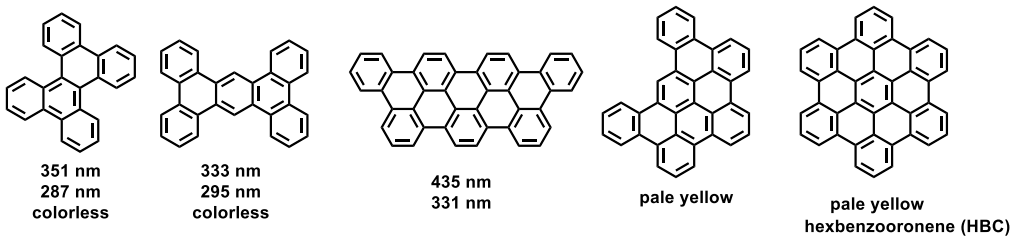

Figure 10. The UV-vis absorption with only the longest wavelengths shown and the color of a few PAHs indicated.

It is interesting to explore origins of the light absorption of PAHs based on the authentic structures observed by AFM imaging. TD-DFT calculations (**Figure 11)** showed some of the compounds to have long wavelength absorption. It can be seen that a few compounds could actually absorb significantly in the visible region. Although some contain heteroatoms (C1.27, C1.36), hydrocarbons alone could also absorb in the visible wavelength. This further confirms the previous analysis that the most stable fully benzenoids are rarely found in petroleum PAHs.

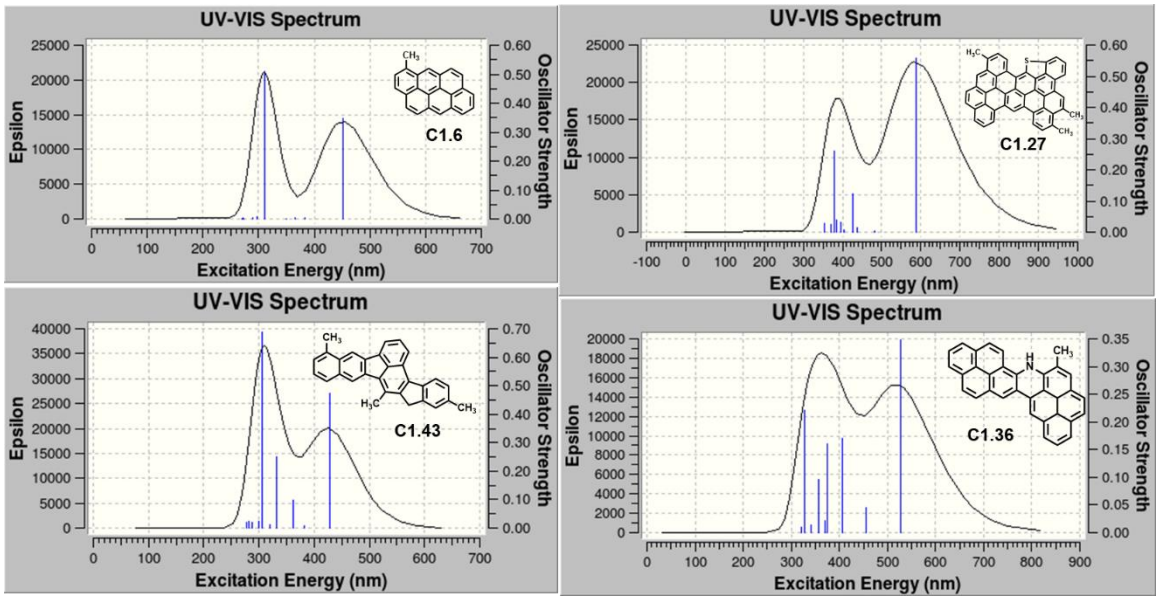

Figure 11. UV-vis spectra predicted by TD DFT calculations on the AFM structures.

Another notable reason could be due to the presence of nonalternant PAHs in asphaltenes. It is well known that nonalternant aromatic molecules have distinctive light absorption spectra. For example, the longest wavelength at which azulene absorbs light is 700 nm whereas the longest for isomeric naphthalene is only 280 nm. By introducing pentagons/heptagons into the aromatic system, the aromatics could reach further into the infrared region, covering the whole UV-vis spectrum. This provides an additional explanations for the black color of petroleum oil, in additional to previously studied very large PAH and their aggregations,[86] heteroatoms, metals, free radicals, and Urbach tail,[83] etc. These studies on understanding the spectrum of light absorption could help take advantage of these heavy petroleum species for optical applications.

4.7. The location of double bond character

It is not only important to know the overall stability of the molecules based on aromaticity, but also important to understand the local reactive sites within a molecule. Quantifying bonding order provided such a means to understand the olefinic character of certain bonds in aromatic compounds. As mentioned above, aromaticity can be considered as the extra stability gained at the loss of olefinic reactivities, such as the electrophilic substitution reaction of benzene instead of addition reaction of alkenes. Bond order analysis provides a convenient way to compare the bonds within the same molecule and among different structures. The bond order calculated form natural orbital analysis by DFT is presented in **Figure 12**.

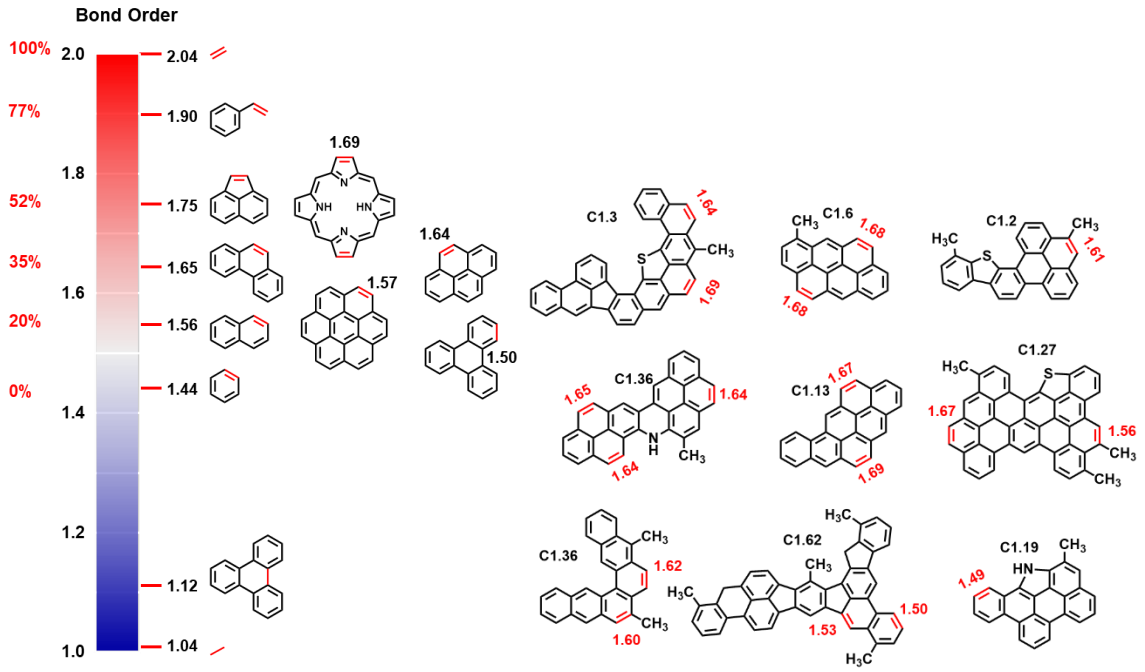

Figure 12. Computation of bond order with natural molecular orbitals. The scale of bond order at left is calibrated by some aromatic molecules with calculated bond order shown for the specific bond location indicated in red; and (right) in each molecule among all bonds only bonds with highest bond order are shown in red. Reprinted with permission from Ref. [40]. Copyright 2018 American Chemical Society.

Benchmarked by alkane (bond order 1 in ethane) and alkene (bond order 2 in ethylene), the bond order of benzene is 1.44, which can be considered as a reference for aromaticity. Naphthalene (bond order 1.56) and phenanthrene (1.65) have increased partial double bond character, especially the CC bond at the 9,10-poition of phenanthrene has been considered as a *true* double bond because it can participate in most olefinic reactions. Therefore, a bond order above 1.65 can be considered as an *olefinic bond* in PAHs. The bond order of the olefinic bonds in acenaphthene (1.75) and styrene (1.90) have higher bond orders. Therefore, it can be seen that bond orders in PAHs span the whole range of bond orders, from single to double bond. Certain locations in PAHs can not only increase bond order to reach that of olefins, but also can decrease and reach that of single bond (e.g., 1.12 in triphenylene).

Based on this, it is important to analyze the detailed structures from AFM imaging. It can be seen that most molecules have a few bonds with significant double bond order, although it is generally believed that naturally occurring petroleum molecules are devoid of olefins (alkenes) and only composed of aliphatic (alkanes) and aromatic moieties. In rare cases where olefins were detected, it was eventually found that they were generated from special external sources (e.g. radiolysis).[89] From this study, we can conclude that although conventional olefins may not be present in petroleum (e.g., by the criteria of olefinic region in NMR), partially enriched double bonds are ubiquitous in petroleum as soon as PAHs are present. Recognition of this results is important in understanding the reactivities of aromatic molecules in petroleum and in the design of reactions.

5. Conclusions

In this chapter, the molecular characterization for organic molecules was reviewed, with a focus on new characterization tools using the molecular imaging technique at atomic resolution. Noncontact atomic force microscopy (nc-AFM) was introduced and its applications to characterize the unknown molecular structure in petroleum asphaltenes and heavy oils have been reviewed. A systemic analysis on these structures from AFM imaging is presented. PAHs can be categorized as alternant and nonalternant hydrocarbons, and both are present in these AFM imaged structures. The presence of nonalternant PAHs (containing a five-membered or other odd-number carbon rings) are especially worth noting, because their abundance in petroleum was not clear and not well studied. Aromaticity analysis indicates that local aromaticity is maximized and these five-membered rings function as a divider within PAH structures, which is also evident from electrostatic potential surfaces. Clar's theory was used to analyze the relative stability of different kinds of PAHs by classifying them into four groups. It was found that, while the most stable and least stable type of PAHs are rare, the two intermediate kinds are most abundant. Finally, the partial double bond of PAHs was revealed by quantitative bond order analysis and showed certain sites of a PAH could attain significant double bond character, enabling them be the reactive sites participating in chemical reactions.

AUTHOR INFORMATION

Corresponding Author

*Yunlong Zhang yunlong.zhang@exxonmobil.com Tel: 908-335-2792

ACKNOWLEDGMENT

The author would like to acknowledge ExxonMobil Research and Engineering Company for the support of this research and release of this work. Discussions with many colleagues and collaborators, especially with Leo Gross and Bruno Schuler of IBM research (Zurich) are gratefully acknowledged. Revision of this draft by Michael Siskin and Steven P. Rucker are gratefully acknowledged.

REFERENCES

1. Hoffmann, R., Foreward to the monograph. In *Determination of the Geometrical Structures of Free Molecules*, Vilkov, L. V.; Mastryukov, V. S.; Sadova, N. I., Eds. Mir Publishers: Moscow, 1993.
2. Kekulé, A., Sur la constitution des substances aromatiques (in French). *Bull. Soc. Chim.* **1865,** *3*, 98.
3. Silverstein, R. M.; Webster, F. X.; Kiemle, D. J.; Bryce, D. L., *Spectrometric identification of organic compounds*. John Wiley & Sons: Hoboken, NJ, 2015.
4. Seeman, J. I., On the Relationship between Classical Structure Determination and Retrosynthetic Analysis/Total Synthesis. *Isr. J. Chem.* **2018,** *58* (1-2), 28-44.
5. Feynman, R. P., There's plenty of room at the bottom. In *Feynman and computation*, Anthony, J. G. H., Ed. Perseus Books: 1999, pp 63-76.
6. Rust, M. J.; Bates, M.; Zhuang, X., Sub-diffraction-limit imaging by stochastic optical reconstruction microscopy (STORM). *Nat. Methods* **2006,** *3*, 793-796.

7. Thompson, M. A.; Lew, M. D.; Moerner, W. E., Extending Microscopic Resolution with Single-Molecule Imaging and Active Control. *Annual Review of Biophysics* **2012,** *41* (1), 321-342.
8. Moerner, W. E., New directions in single-molecule imaging and analysis. *Proc. Natl. Acad. Sci. U.S.A.* **2007,** *104* (31), 12596-12602.
9. Renaud, J.-P.; Chari, A.; Ciferri, C.; Liu, W.-t.; Rémigy, H.-W.; Stark, H.; Wiesmann, C., Cryo-EM in drug discovery: achievements, limitations and prospects. *Nat. Rev. Drug Discovery* **2018,** *17*, 471.
10. Fernandez-Leiro, R.; Scheres, S. H. W., Unravelling biological macromolecules with cryo-electron microscopy. *Nature* **2016,** *537*, 339.
11. Evans, J. E.; Hetherington, C.; Kirkland, A.; Chang, L.-Y.; Stahlberg, H.; Browning, N., Low-dose aberration corrected cryo-electron microscopy of organic specimens. *Ultramicroscopy* **2008,** *108* (12), 1636-1644.
12. Jiang, X.; Greer, D. R.; Kundu, J.; Ophus, C.; Minor, A. M.; Prendergast, D.; Zuckermann, R. N.; Balsara, N. P.; Downing, K. H., Imaging Unstained Synthetic Polymer Crystals and Defects on Atomic Length Scales Using Cryogenic Electron Microscopy. *Macromolecules* **2018,** *51* (19), 7794-7799.
13. Erni, R.; Rossell, M. D.; Kisielowski, C.; Dahmen, U., Atomic-Resolution Imaging with a Sub-50-pm Electron Probe. *Phys. Rev. Lett.* **2009,** *102* (9), 96101-96104.
14. Girit, Ç. Ö.; Meyer, J. C.; Erni, R.; Rossell, M. D.; Kisielowski, C.; Yang, L.; Park, C.-H.; Crommie, M. F.; Cohen, M. L.; Louie, S. G.; Zettl, A., Graphene at the Edge: Stability and Dynamics. *Science* **2009,** *323*, 1705-1708.
15. Jones, C. G.; Martynowycz, M. W.; Hattne, J.; Fulton, T. J.; Stoltz, B. M.; Rodriguez, J. A.; Nelson, H. M.; Gonen, T., The CryoEM Method MicroED as a Powerful Tool for Small Molecule Structure Determination. *ACS Cent. Sci.* **2018,** *4* (11), 1587–1592.
16. Kunde, T.; Schmidt, B. M., Microcrystal Electron Diffraction (MicroED) for Small-Molecule Structure Determination. *Angew. Chem., Int. Ed.* **2018**, 10.1002/anie.201813215, Ahead of Print.
17. Gross, L.; Mohn, F.; Moll, N.; Liljeroth, P.; Meyer, G., The Chemical Structure of a Molecule Resolved by Atomic Force Microscopy. *Science* **2009,** *325*, 1110-1114.
18. Gross, L.; Mohn, F.; Moll, N.; Schuler, B.; Criado, A.; Guitian, E.; Pena, D.; Gourdon, A.; Meyer, G., Bond-Order Discrimination by Atomic Force Microscopy. *Science* **2012,** *337*, 1326-1329.
19. Binnig, G.; Rohrer, H.; Gerber, C.; Weibel, E., Tunneling through a controllable vacuum gap. *Appl. Phys. Lett.* **1982,** *40* (2), 178-180.
20. Binnig, G.; Quate, C. F.; Gerber, C., Atomic Force Microscope. *Phys. Rev. Lett.* **1986,** *56* (9), 930-933.
21. Jalili, N.; Laxminarayana, K., A review of atomic force microscopy imaging systems: application to molecular metrology and biological sciences. *Mechatronics* **2004,** *14* (8), 907-945.
22. Giessibl, F. J., High-speed force sensor for force microscopy and profilometry utilizing a quartz tuning fork. *Appl. Phys. Lett.* **1998,** *73* (26), 3956-3958.
23. Hapala, P.; Kichin, G.; Wagner, C.; Tautz, F. S.; Temirov, R.; Jelinek, P., Mechanism of high-resolution STM/AFM imaging with functionalized tips. *Phys. Rev. B Condens. Matter Mater. Phys.* **2014,** *90* (8), 085421-085429.
24. Hapala, P.; Temirov, R.; Tautz, F. S.; Jelinek, P., Origin of High-Resolution IETS-STM Images of Organic Molecules with Functionalized Tips. *Phys Rev Lett* **2014,** *113* (22), 226101.

25. Shiotari, A.; Sugimoto, Y., Ultrahigh-resolution imaging of water networks by atomic force microscopy. *Nat. Commun.* **2017,** *8*, 14313.
26. Gross, L.; Mohn, F.; Moll, N.; Meyer, G.; Ebel, R.; Abdel-Mageed, W. M.; Jaspars, M., Organic structure determination using atomic-resolution scanning probe microscopy. *Nat. Chem.* **2010,** *2* (10), 821-825.
27. de Oteyza, D. G.; Gorman, P.; Chen, Y.-C.; Wickenburg, S.; Riss, A.; Mowbray, D. J.; Etkin, G.; Pedramrazi, Z.; Tsai, H.-Z.; Rubio, A.; Crommie, M. F.; Fischer, F. R., Direct Imaging of Covalent Bond Structure in Single-Molecule Chemical Reactions. *Science* **2013,** *340* (6139), 1434-1437.
28. Hla; Bartels; Meyer; Rieder, Inducing all steps of a chemical reaction with the scanning tunneling microscope tip: towards single molecule engineering. *Phys. Rev. Lett.* **2000,** *85* (13), 2777-2780.
29. Iwata, K.; Yamazaki, S.; Mutombo, P.; Hapala, P.; Ondracek, M.; Jelinek, P.; Sugimoto, Y., Chemical structure imaging of a single molecule by atomic force microscopy at room temperature. *Nat. Commun.* **2015,** *6*, 7766-7773.
30. Zhang, J.; Chen, P.; Yuan, B.; Ji, W.; Cheng, Z.; Qiu, X., Real-space identification of intermolecular bonding with atomic force microscopy. *Science* **2013,** *342*, 611-614.
31. Bartels, L.; Meyer, G.; Rieder, K. H., Controlled vertical manipulation of single CO molecules with the scanning tunneling microscope: A route to chemical contrast. *Appl. Phys. Lett.* **1997,** *71* (2), 213-215.
32. Gross, L.; Schuler, B.; Pavlicek, N.; Fatayer, S.; Majzik, Z.; Moll, N.; Pena, D.; Meyer, G., Atomic Force Microscopy for Molecular Structure Elucidation. *Angew. Chem. Int. Ed. Engl.* **2018,** *57* (15), 3888-3908.
33. Schuler, B.; Zhang, Y.; Collazos, S.; Fatayer, S.; Meyer, G.; Perez, D.; Guitian, E.; Harper, M. R.; Kushnerick, J. D.; Pena, D.; Gross, L., Characterizing aliphatic moieties in hydrocarbons with atomic force microscopy. *Chem. Sci.* **2017,** *8* (3), 2315-2320.
34. Zhang, Y.; Schuler, B.; Fatayer, S.; Gross, L.; Harper, M. R.; Kushnerick, J. D., Understanding the Effects of Sample Preparation on the Chemical Structures of Petroleum Imaged with Noncontact Atomic Force Microscopy. *Ind. Eng. Chem. Res.* **2018,** *57* (46), 15935-15941.
35. Hinaut, A.; Meier, T.; Pawlak, R.; Feund, S.; Johr, R.; Kawai, S.; Glatzel, T.; Decurtins, S.; Mullen, K.; Narita, A.; Liu, S.-X.; Meyer, E., Electrospray deposition of structurally complex molecules revealed by atomic force microscopy. *Nanoscale* **2018,** *10* (3), 1337-1344.
36. Schuler, B.; Meyer, G.; Pena, D.; Mullins, O. C.; Gross, L., Unraveling the Molecular Structures of Asphaltenes by Atomic Force Microscopy. *J. Am. Chem. Soc.* **2015,** *137* (31), 9870-9876.
37. Schuler, B.; Fatayer, S.; Meyer, G.; Rogel, E.; Moir, M.; Zhang, Y.; Harper, M. R.; Pomerantz, A. E.; Bake, K. D.; Witt, M.; Pena, D.; Kushnerick, J. D.; Mullins, O. C.; Ovalles, C.; van den Berg, F. G. A.; Gross, L., Heavy Oil Based Mixtures of Different Origins and Treatments Studied by Atomic Force Microscopy. *Energy Fuels* **2017,** *31* (7), 6856-6861.
38. Fatayer, S.; Poddar, N. B.; Quiroga, S.; Schulz, F.; Schuler, B.; Kalpathy, S. V.; Meyer, G.; Perez, D.; Guitian, E.; Pena, D.; Wornat, M. J.; Gross, L., Atomic Force Microscopy Identifying Fuel Pyrolysis Products and Directing the Synthesis of Analytical Standards. *J. Am. Chem. Soc.* **2018,** *140* (26), 8156-8161.
39. Fatayer, S.; Coppola, A. I.; Schulz, F.; Walker, B. D.; Broek, T. A.; Meyer, G.; Druffel, E. R. M.; McCarthy, M.; Gross, L., Direct Visualization of Individual Aromatic Compound

Structures in Low Molecular Weight Marine Dissolved Organic Carbon. *Geophys. Res. Lett.* **2018,** *45* (11), 5590-5598.
40. Zhang, Y., Nonalternant Aromaticity and Partial Double Bond in Petroleum Molecules Revealed: Theoretical Understanding of Polycyclic Aromatic Hydrocarbons Obtained by Non-contact Atomic Force Microscopy. *Energy Fuels* **2018,** *ASAP*, DOI: 10.1021/acs.energyfuels.8b03284.
41. Frisch, M. J.; Trucks, G. W.; Schlegel, H. B.; Scuseria, G. E.; Robb, M. A.; Cheeseman, J. R.; Scalmani, G.; Barone, V.; Mennucci, B.; Petersson, G. A.; Nakatsuji, H.; Caricato, M.; Li, X.; Hratchian, H. P.; Izmaylov, A. F.; Bloino, J.; Zheng, G.; Sonnenberg, J. L.; Hada, M.; Ehara, M.; Toyota, K.; Fukuda, R.; Hasegawa, J.; Ishida, M.; Nakajima, T.; Honda, Y.; Kitao, O.; Nakai, H.; Vreven, T.; Montgomery, J. A.; Peralta, J. E.; Ogliaro, F.; Bearpark, M.; Heyd, J. J.; Brothers, E.; Kudin, K. N.; Staroverov, V. N.; Kobayashi, R.; Normand, J.; Raghavachari, K.; Rendell, A.; Burant, J. C.; Iyengar, S. S.; Tomasi, J.; Cossi, M.; Rega, N.; Millam, J. M.; Klene, M.; Knox, J. E.; Cross, J. B.; Bakken, V.; Adamo, C.; Jaramillo, J.; Gomperts, R.; Stratmann, R. E.; Yazyev, O.; Austin, A. J.; Cammi, R.; Pomelli, C.; Ochterski, J. W.; Martin, R. L.; Morokuma, K.; Zakrzewski, V. G.; Voth, G. A.; Salvador, P.; Dannenberg, J. J.; Dapprich, S.; Daniels, A. D.; Farkas; Foresman, J. B.; Ortiz, J. V.; Cioslowski, J.; Fox, D. J. *Gaussian 09, Revision B.01*, Wallingford CT, 2009.
42. Becke, A. D., Density-functional thermochemistry. III. The role of exact exchange. *J. Chem. Phys.* **1993,** *98* (7), 5648-5652.
43. Lee, C.; Yang, W.; Parr, R. G., Development of the Colle-Salvetti correlation-energy formula into a functional of the electron density. *Physical Review B* **1988,** *37* (2), 785-789.
44. Schleyer, P. v. R.; Maerker, C.; Dransfeld, A.; Jiao, H.; van Eikema Hommes, N. J. R., Nucleus-independent chemical shifts: a simple and efficient aromaticity probe. *J. Am. Chem. Soc.* **1996,** *118* (26), 6317-6318.
45. Wiberg, K. B., Properties of Some Condensed Aromatic Systems. *J. Org. Chem.* **1997,** *62* (17), 5720-5727.
46. Foster, J. P.; Weinhold, F., Natural hybrid orbitals. *J. Am. Chem. Soc.* **1980,** *102* (24), 7211-7218.
47. Glendening, E. D.; Reed, A. E.; Carpenter, B. K.; Weinhold, F. *NBO Version 3.1*.
48. Mayer, I., Bond order and valence indices: A personal account. *J. Comput. Chem.* **2007,** *28* (1), 204-221.
49. Coulson, C. A.; Rushbrooke, G. S., The method of molecular orbitals. *Proc. Cambridge Philos. Soc.* **1940,** *36*, 193-200.
50. Yen, T. F.; Erdman, J. G.; Saraceno, A. J., Investigation of the nature of free radicals in petroleumasphaltenes and related substances by electron spin resonance. *Anal. Chem.* **1962,** *34*, 694-700.
51. Biktagirov, T. B.; Gafurov, M. R.; Volodin, M. A.; Mamin, G. V.; Rodionov, A. A.; Izotov, V. V.; Vakhin, A. V.; Isakov, D. R.; Orlinskii, S. B., Electron Paramagnetic Resonance Study of Rotational Mobility of Vanadyl Porphyrin Complexes in Crude Oil Asphaltenes: Probing the Effect of Thermal Treatment of Heavy Oils. *Energy Fuels* **2014,** *28* (10), 6683-6687.
52. Trukhan, S. N.; Kazarian, S. G.; Martyanov, O. N., Electron Spin Resonance of Slowly Rotating Vanadyls-Effective Tool to Quantify the Sizes of Asphaltenes in Situ. *Energy Fuels* **2017,** *31* (1), 387-394.
53. Vöge, M.; Guttmann, A. J.; Jensen, I., On the Number of Benzenoid Hydrocarbons. *J. Chem. Inf. Comput. Sci.* **2002,** *42* (3), 456-466.

54. Dias, J. R., A periodic table for polycyclic aromatic hydrocarbons. Isomer enumeration of fused polycyclic aromatic hydrocarbons. Part I. *J. Chem. Inf. Comput. Sci.* **1982,** *22* (1), 15-22.
55. Dias, J. R., Periodic table for polycyclic aromatic hydrocarbons. 2. Polycyclic aromatic hydrocarbons containing tetragonal, pentagonal, heptagonal, and octagonal rings. *J. Chem. Inf. Comput. Sci.* **1982,** *22* (3), 139-152.
56. Dias, J. R., A periodic table for polycyclic aromatic hydrocarbons. Part 3. Enumeration of all the polycyclic conjugated isomers of pyrene having ring sizes ranging from 3 to 9. *MATCH* **1983,** *14*, 83-138.
57. Dias, J. R., Isomer enumeration of nonradical strictly peri-condensed polycyclic aromatic hydrocarbons. *Can. J. Chem.* **1984,** *62* (12), 2914-2922.
58. Dias, J. R., A periodic table for polycyclic aromatic hydrocarbons. IV. Isomer enumeration of polycyclic conjugated hydrocarbons. 2. *J. Chem. Inf. Comput. Sci.* **1984,** *24* (3), 124-135.
59. Dias, J. R., A periodic table for polycyclic aromatic hydrocarbons. V. 1-Factorable, 2-factorable, and Dewar graph structures associated with benzenoid hydrocarbons. *J. Macromol. Sci., Chem.* **1985,** *A22* (3), 335-360.
60. Dias, J. R., Isomer enumeration of practical benzenoids. *J. Math. Chem.* **2008,** *44* (3), 711-724.
61. Dias, J. R., Structure/formula informatics of isomeric sets of fluoranthenoid/fluorenoid and indacenoid hydrocarbons. *J. Math. Chem.* **2010,** *48* (2), 313-329.
62. Dias, J. R., Strain-Free Total Resonant Sextet Benzenoids and Their Antisextet Dualists and Retro-Leapfrogs. *J. Chem. Inf. Model.* **2007,** *47* (1), 20-24.
63. El Bakouri, O.; Poater, J.; Feixas, F.; Solà, M., Exploring the validity of the Glidewell–Lloyd extension of Clar's π-sextet rule: assessment from polycyclic conjugated hydrocarbons. *Theor. Chem. Acc.* **2016,** *135* (8), 205-217.
64. Klevens, H. B.; Platt, J. R., Spectral Resemblances of Cata-Condensed Hydrocarbons. *J. Chem. Phys.* **1949,** *17*, 470.
65. Randić, M., Aromaticity of Polycyclic Conjugated Hydrocarbons. *Chem. Rev.* **2003,** *103* (9), 3449-3606.
66. Clar, E., *The Aromatic Sextet*. Wiley: New York, 1972.
67. Houk, K. N.; Lee, P. S.; Nendel, M., Polyacene and Cyclacene Geometries and Electronic Structures: Bond Equalization, Vanishing Band Gaps, and Triplet Ground States Contrast with Polyacetylene. *J. Org. Chem.* **2001,** *66* (16), 5517-5521.
68. Mondal, R.; Tonshoff, C.; Khon, D.; Neckers, D. C.; Bettinger, H. F., Synthesis, Stability, and Photochemistry of Pentacene, Hexacene, and Heptacene: A Matrix Isolation Study. *J. Am. Chem. Soc.* **2009,** *131* (40), 14281-14289.
69. Krüger, J.; Eisenhut, F.; Skidin, D.; Lehmann, T.; Ryndyk, D. A.; Cuniberti, G.; García, F.; Alonso, J. M.; Guitián, E.; Pérez, D.; Peña, D.; Trinquier, G.; Malrieu, J.-P.; Moresco, F.; Joachim, C., Electronic Resonances and Gap Stabilization of Higher Acenes on a Gold Surface. *ACS Nano* **2018,** *12* (8), 8506-8511.
70. Poater, J.; Poater, J.; Duran, M.; Sola, M., Aromaticity Determines the Relative Stability of Kinked vs. Straight Topologies in Polycyclic Aromatic Hydrocarbons. *Front Chem* **2018,** *6*, 561.
71. Dias, J. R., The Most Stable Class of Benzenoid Hydrocarbons-New Topological Correlations of Strain-Free Total Resonant Sextet Benzenoids. *J. Chem. Inf. Comput. Sci.* **2004,** *44* (4), 1210-1220.

72. IUPAC. Compendium of Chemical Terminology, 2nd ed. (the "Gold Book"). McNaught, A. D.; Wilkinson, A., Eds. Blackwell Scientific Publications, Oxford: https://doi.org/10.1351/goldbook, 1997.
73. Frenking, G.; Krapp, A., Unicorns in the world of chemical bonding models. *J. Comput. Chem.* **2006,** *28* (1), 15-24.
74. Krygowski, T. M.; Cyrański, M., Separation of the energetic and geometric contributions to the aromaticity. Part IV. A general model for the π-electron systems. *Tetrahedron* **1996,** *52* (30), 10255-10264.
75. Krygowski, T. M.; Cyrański, M. K., Structural Aspects of Aromaticity. *Chem. Rev.* **2001,** *101* (5), 1385-1420.
76. Schleyer, P. v. R., Introduction: Aromaticity. *Chem. Rev.* **2001,** *101* (5), 1115-1118.
77. Ruiz-Morales, Y., HOMO-LUMO Gap as an Index of Molecular Size and Structure for Polycyclic Aromatic Hydrocarbons (PAHs) and Asphaltenes: A Theoretical Study. I. *J. Phys. Chem. A* **2002,** *106* (46), 11283-11308.
78. Ruiz-Morales, Y., The Agreement between Clar Structures and Nucleus-Independent Chemical Shift Values in Pericondensed Benzenoid Polycyclic Aromatic Hydrocarbons: An Application of the Y-Rule. *J. Phys. Chem. A* **2004,** *108* (49), 10873-10896.
79. Ruiz-Morales, Y., Aromaticity in pericondensed cyclopenta-fused polycyclic aromatic hydrocarbons determined by density functional theory nucleus-independent chemical shifts and the Y-rule - Implications in oil asphaltene stability. *Can. J. Chem.* **2009,** *87* (10), 1280-1295.
80. Glidewell, C.; Lloyd, D., Mndo study of bond orders in some conjugated BI- and tri-cyclic hydrocarbons. *Tetrahedron* **1984,** *40* (21), 4455-4472.
81. Aihara, J.-i.; Makino, M.; Sakamoto, K., Superaromatic Stabilization Energy as a Novel Local Aromaticity Index for Polycyclic Aromatic Hydrocarbons. *J. Phys. Chem. A* **2013,** *117* (40), 10477-10488.
82. Lovas, F. J.; McMahon, R. J.; Grabow, J. U.; Schnell, M.; Mack, J.; Scott, L. T.; Kuczkowski, R. L., Interstellar chemistry: a strategy for detecting polycyclic aromatic hydrocarbons in space. *J. Am. Chem. Soc.* **2005,** *127* (12), 4345-4349.
83. Ruiz-Morales, Y.; Wu, X.; Mullins, O. C., Electronic Absorption Edge of Crude Oils and Asphaltenes Analyzed by Molecular Orbital Calculations with Optical Spectroscopy. *Energy Fuels* **2007,** *21* (2), 944-952.
84. Ruiz-Morales, Y.; Mullins, O. C., Measured and Simulated Electronic Absorption and Emission Spectra of Asphaltenes. *Energy Fuels* **2009,** *23* (3), 1169-1177.
85. Juyal, P.; McKenna, A. M.; Yen, A.; Rodgers, R. P.; Reddy, C. M.; Nelson, R. K.; Andrews, A. B.; Atolia, E.; Allenson, S. J.; Mullins, O. C.; Marshall, A. G., Analysis and Identification of Biomarkers and Origin of Color in a Bright Blue Crude Oil. *Energy Fuels* **2011,** *25* (1), 172-182.
86. Mullins, O. C.; Mitra-Kirtley, S.; Zhu, Y., The Electronic Absorption Edge of Petroleum. *Appl. Spectrosc.* **1992,** *46* (9), 1405-1411.
87. Kurik, M. V., Urbach rule. *physica status solidi (a)* **1971,** *8* (1), 9-45.
88. Wasserfallen, D.; Kastler, M.; Pisula, W.; Hofer, W. A.; Fogel, Y.; Wang, Z.; Muellen, K., Suppressing Aggregation in a Large Polycyclic Aromatic Hydrocarbon. *J. Am. Chem. Soc.* **2006,** *128* (4), 1334-1339.
89. Curiale, J. A.; Frolov, E. B., Occurrence and origin of olefins in crude oils. A critical review. *Org. Geochem.* **1998,** *29* (1), 397-408.